Synthesis and Synchrotron Light-Induced Luminescence of ZnO Nanostructures: Nanowires, Nanoneedles, Nanoflowers, and Tubular Whiskers

X. H. Sun,[†] S. Lam,[†] T. K. Sham,*[,†] F. Heigl,[‡] A. Jürgensen,[‡] and N. B. Wong*[,§]

Department of Chemistry, University of Western Ontario, London, Canada N6A 5B7, Canadian Synchrotron Radiation Facility, Synchrotron Radiation Center, University of Wisconsin−Madison, Stoughton, Wisconsin 53589-3097, and Department of Biology and Chemistry, City University of Hong Kong, Hong Kong

Received: November 5, 2004; In Final Form: December 6, 2004

ZnO nanostructures, including single-crystal nanowires, nanoneedles, nanoflowers, and tubular whiskers, have been fabricated at a modestly low temperature of 550 °C via the oxidation of metallic Zn powder without a metal catalyst. Specific ZnO nanostructures can be obtained at a specific temperature zone in the furnace depending on the temperature and the pressure of oxygen. Scanning electron microscopy (SEM), high-resolution transmission electron microscopy (HRTEM), and X-ray diffraction (XRD) studies show that ZnO nanostructures thus prepared are single crystals with a wurtzite structure. X-ray excited optical luminescence (XEOL) from the ZnO nanostructures show noticeable morphology-dependent luminescence. Specifically, ZnO nanowires of around 15 nm in diameter emit the strongest green light. The morphology of these nanostructures, their XEOL, and the implication of the results will be discussed.

Introduction

Semiconductor nanomaterials have received broad attention partly because they exhibit interesting electronic and optical properties intrinsically associated with their low dimensionality and the quantum confinement effect, and partly because they represent critical components in potential nanoscale device applications. Among these materials, ZnO is a promising candidate for optoelectronics and piezoelectricity effects due to a wide band-gap (3.37 eV), a large exciton binding energy (60 meV) at room temperature, and its noncentrosymmetry in the wurtzite structure.[1] A large variety of ZnO nanostructures, such as nanowires (nanorods),[2−4] nanotube,[5−7] nanobelts,[8] nanocombs,[9] nanorings, nanosprings,[10] nanopropellers,[11] and tetrapods-like nanostructures,[12,13] have been realized. Preparation techniques include thermal evaporation,[2,7−11] chemical vapor deposition (CVD),[5] and solution-phase.[4] The diverse morphologies of ZnO nanostructures are desirable for potential applications in novel nanodevices such as UV laser,[2] field-effect transistors,[14] field emitter,[15] nanosensors,[16] nanoresonators,[17] and nanocantilevers.[18] Here, we present a simple approach to obtain different ZnO nanostructures such as single-crystal nanowires, nanoneedles, nanoflowers, and tubular whiskers via controlled oxidation of metallic Zn powder without the use of any metal catalyst at a modestly low temperature of ∼550 °C. We show that specific ZnO nanostructures can be obtained at a specific temperature zone in the furnace by controlling the temperature and the partial pressure of oxygen and Zn. X-ray excited optical luminescence (XEOL) from these ZnO nanostructures shows noticeable morphology-dependent luminescence associated with crystallinity and surface roughness.

* Corresponding authors. E-mail: (T.K.S.) sham@uwo.ca; (N.B.W.) bhnbwong@cityu.edu.hk.
[†] University of Western Ontario.
[‡] University of Wisconsin−Madison.
[§] City University of Hong Kong.

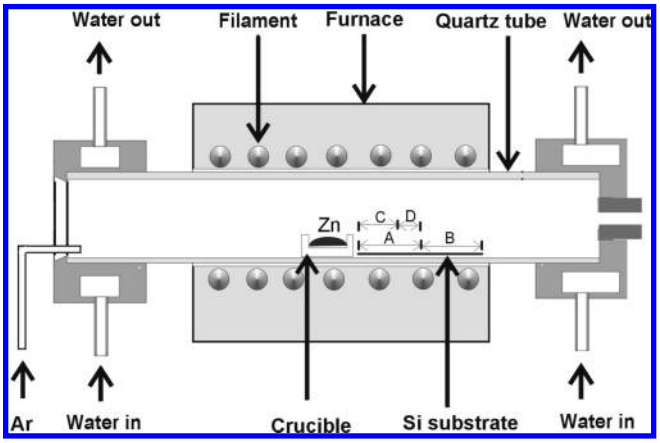

Figure 1. A schematic diagram of the experimental apparatus for growth of ZnO nanostructures by the solid−vapor phase process.

Experimental Section

The ZnO nanostructures were synthesized in a horizontal tube furnace system (Figure 1). A quartz tube was mounted inside a tube furnace. An alumina crucible containing Zn powder (99.9%, Alfa Aesar) was placed at the middle of the high-temperature zone of the furnace. A 9 cm-long silicon wafer cleaned by sonication in ethanol and acetone was placed at a position downstream of the carrier gas. The carrier gas, argon, was introduced at one end of the quartz tube at a flow rate of 100 sccm (standard cubic centimeters per minute), and the other end of the quartz was open to air. The temperature of the furnace was increased to 550 °C and kept at this temperature for 60 min. In another experiment, the Zn partial pressure was reduced by covering the crucible containing the Zn powder with a silicon wafer, restricting its exposure to the carrier gas flow. During the experiment, the temperature at different positions of the silicon substrate in the quartz tube was monitored with a thermal couple. After the reaction, gray- and white-colored products

10.1021/jp044926v CCC: $30.25
Published on Web 01/27/2005

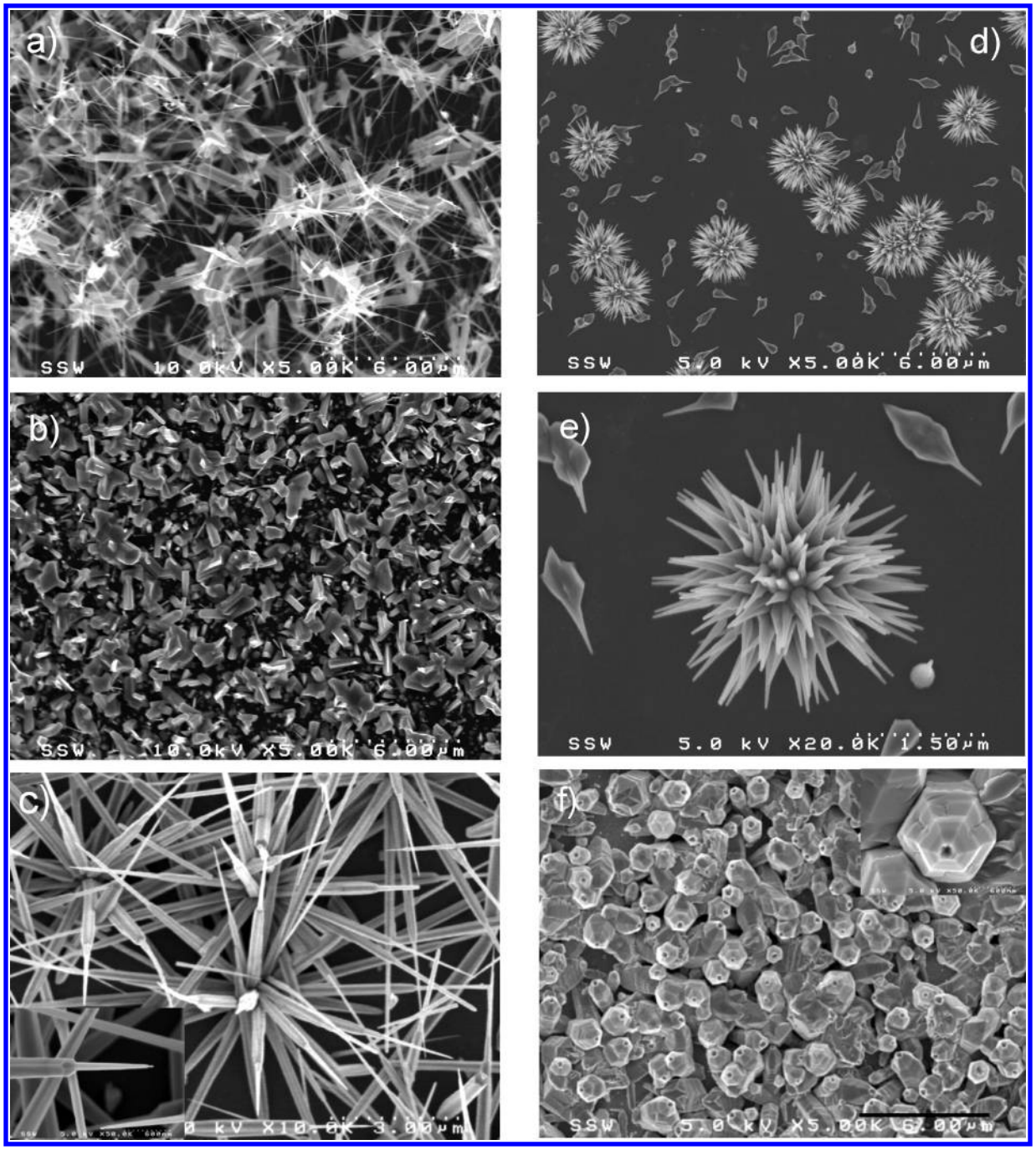

Figure 2. Typical scanning electron microscopy (SEM) images of different ZnO nanostructures obtained at different positions on the Si substrates. (a) ZnO nanowires at "A" zone, (b) ZnO particles at "B" zone, (c) ZnO nanoneedles at "C" zone, (d,e) ZnO nanoflowers at "D" zone, and (f) ZnO tubular whiskers.

were found covering the silicon substrate, of which the temperature was in the range of 420−540 °C. The morphologies and microstructures of the as-synthesized products were characterized by scanning electron microscopy (Hitachi S-4500 FEG), which was equipped with energy-dispersive X-ray spectroscopy (EDS) for composition analyses, transmission electron microscopy (Philips CM10), high-resolution transmission electron microscopy (JEOL 2010F), which was attached with a EDS for single nanostructure composition analyses, and X-ray diffraction (Rigaku, Co Kα radiation, $\lambda = 0.1792$ nm). The X-ray excited optical luminescence (XEOL) of the samples excited with photon energy of 1800 eV was obtained at the Double Crystal Monochromator (DCM) beamline of the Canadian Synchrotron Radiation Facility (CSRF) located at the Synchrotron Radiation Center (SRC), University of Wisconsin−Madison. A JY 100 monochromator was used to monitor the optical photons as described previously.

Results and Discussion

The gray to white film covering the Si substrate is ZnO nanostructures of diverse morphology. Figure 2 shows the scanning electron microscopy (SEM) images of ZnO nanostructures found at different locations of the Si substrates. ZnO nanowires (shown in Figure 2a) were found at the high-temperature zone (500−550 °C), marked as zone "A" in Figure 1, and ZnO particles (Figure 2b) were obtained at the low-temperature zone (420−500 °C, marked as zone "B" in Figure 1). ZnO nanowires were attached to the surface of bigger ZnO particles; that is, each ZnO nanowire has a "root" in the ZnO

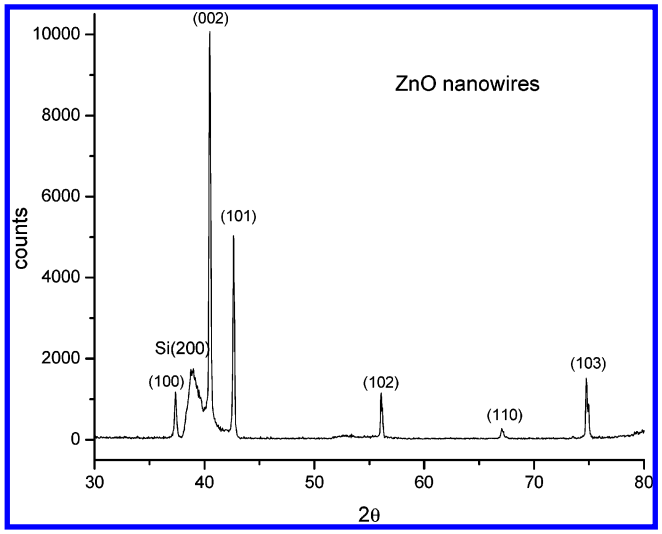

Figure 3. XRD pattern of a ZnO nanowires sample.

particles. The ZnO particles are Zn-rich stoichiometrically from EDX analysis and have a regular hexagonal shape. The ZnO nanowires grew sharper and gradually to several micrometers long from root to tip.

When the Zn source was covered by Si wafer, ZnO nanoneedles (shown in Figure 2c with a single needle shown in the inset at the bottom left corner) were obtained in the high-temperature zone (530−550 °C, marked as zone "C" in Figure 1) and ZnO nanoflowers (Figure 2d, with a single flower structure shown in Figure 2e) were observed in the low-temperature zone (500−530 °C, marked as zone "D" in Figure 1). Tens of ZnO nanoneedles originated from the same "root". Each nanoneedle has a hexagonal tower structure with two or more segments and a sharp tip at the end (inset of Figure 2c). The nanoflower was composed of hundreds of "nanopetals" with tadpole-like structure. There is some nanopetals scattering near the nanoflowers. No product was observed on the area of Si wafer covered on the crucible, although a white powder was observed at the edge where the Si wafer and the crucible came into contact. SEM shows that the white powder was a tubular ZnO whisker (Figure 2f, with a single tube structure shown in the inset). Each ZnO tubular whisker has a hexagonal hollow cone structure. EDX analysis indicates that these nanostructures are composed of zinc and oxygen only. X-ray diffraction (XRD) results confirmed that all of these nanostructures described above have the same ZnO hexagonal wurtzite structure with lattice constants of $a = 0.325$ nm and $c = 0.521$ nm. No diffraction peaks from metallic Zn or other phases were observed. The XRD pattern of the ZnO nanowires sample is shown in Figure 3. The sharp diffraction peaks indicate that the sample is highly crystalline.

Further structural characterization of the ZnO nanowires and ZnO nanoneedles was performed with transmission electron microscopy (TEM). Figure 4a shows the TEM image of several nanowires with similar diameters of around 15 nm and several micrometers in length. For an individual ZnO nanowire, however, its diameter decreases gradually from bottom to the tip. High-resolution TEM (HRTEM) images of the body of a single ZnO nanowire (Figure 4b) and its tip (Figure 4c) show that the ZnO nanowire is structurally uniform and contains no noticeable defects such as dislocations and stacking faults. The lattice spacing of 0.26 nm corresponds to the *d* spacing of the (002) crystal planes of wurtzite ZnO, confirming that the ZnO nanowires have preferential growth orientation in the *c*-axis direction.

Figure 5a shows the TEM image of a single nanoneedle, which has an 80 nm-wide base segment and a ~2 μm-long upper segment with a 10 nm-wide tip. Electron diffraction patterns taken from the different area (base segment, body of the upper segment, and tip) of the single nanoneedle show exactly the same patterns (inset of Figure 5a) and can be indexed with the wurtzite lattice. This result shows that the whole needle is a single crystal with a wurtzite structure. HRTEM images of the tip, body of the upper segment, and connecting part between the upper segment and the base segment (Figure 5b, c, and d), respectively, also show that the nanoneedle is a single crystal without any dislocations and stacking faults. Furthermore, the lattice spacing of 0.26 and 0.52 nm corresponds to the *d* spacing of (002) and (001) crystal planes of wurtzite ZnO, respectively. This indicates that the [001] direction is the preferred growth direction of the ZnO nanoneedles.

Because no catalyst was used and detected in the growth process and the products, respectively, we attribute the growth process of ZnO nanostructures in our experiments to the vapor−solid (VS) process[19] rather than the more common catalyst-assisted vapor−liquid−solid (VLS) process.[20] The ZnO nanostructures were formed on the silicon substrate through a simple chemical reaction:

$$\mathrm{Zn\ (g)} + {}^{1}/_{2}\mathrm{O_2\ (g)} \rightarrow \mathrm{ZnO}$$

Zn atoms were continuously evaporated from the pure Zn powder during heating and oxidized or partially oxidized to ZnO_x ($x \leq 1$) molecules or clusters during the transport onto the Si substrate by the carrier gas. The detailed mechanism for the formation of different morphology of ZnO nanostructures under our experimental condition is not well understood and needs further study. We believe that the partial pressures of zinc and oxygen and the growth temperature are two key factors. It should be noted that, at constant temperature, the Zn vapor pressure is constant while the oxygen partial pressure decreased gradually when the carrier gas began to flow. This can explain the converging behavior of the growth of both the nanowire and the nanoneedle.

In principle, the rates of nucleation and growth influence the morphology of the crystals. It is recognized that oxygen concentration (partial pressure) is an important factor to the rate of nucleation and growth of ZnO crystals[21] and a low oxygen concentration slows the rate. Thus, a low oxygen partial pressure is desirable for the nanostructure growth. Yan et al. found that the shape control of ZnO terapods can be achieved by tuning the oxygen partial pressure. They found that they could increase the diameter of the legs of the tetrapods by increasing the oxygen partial pressure.[12] In our open-end quartz tube, oxygen supply is limited because oxygen is being slowly but constantly perched and the oxygen partial pressure has a gradient in the direction of the flow of the carrier gas. In the ZnO nanowire growth, the Zn source was entirely exposed to the Ar flow. Thus, the ratio of Zn to oxygen pressure is higher than the condition for the formation of nanoneedles and nanoflowers in which the Zn source was covered with a silicon wafer. Thus, the nucleation and growth rates for ZnO were slower in the former, resulting in finer nanowire growth. Furthermore, a Zn-rich atmosphere (Zn or ZnO_x ($x < 1$)) has been shown to be favorable for the nucleation of ZnO nanowires.[22] Zn-rich ZnO particles have been observed in the region where ZnO nanowires grew from the surfaces of those particles. A quantitative study of the effect of oxygen partial pressure on the ZnO nanostructure morphologies is needed in future studies.

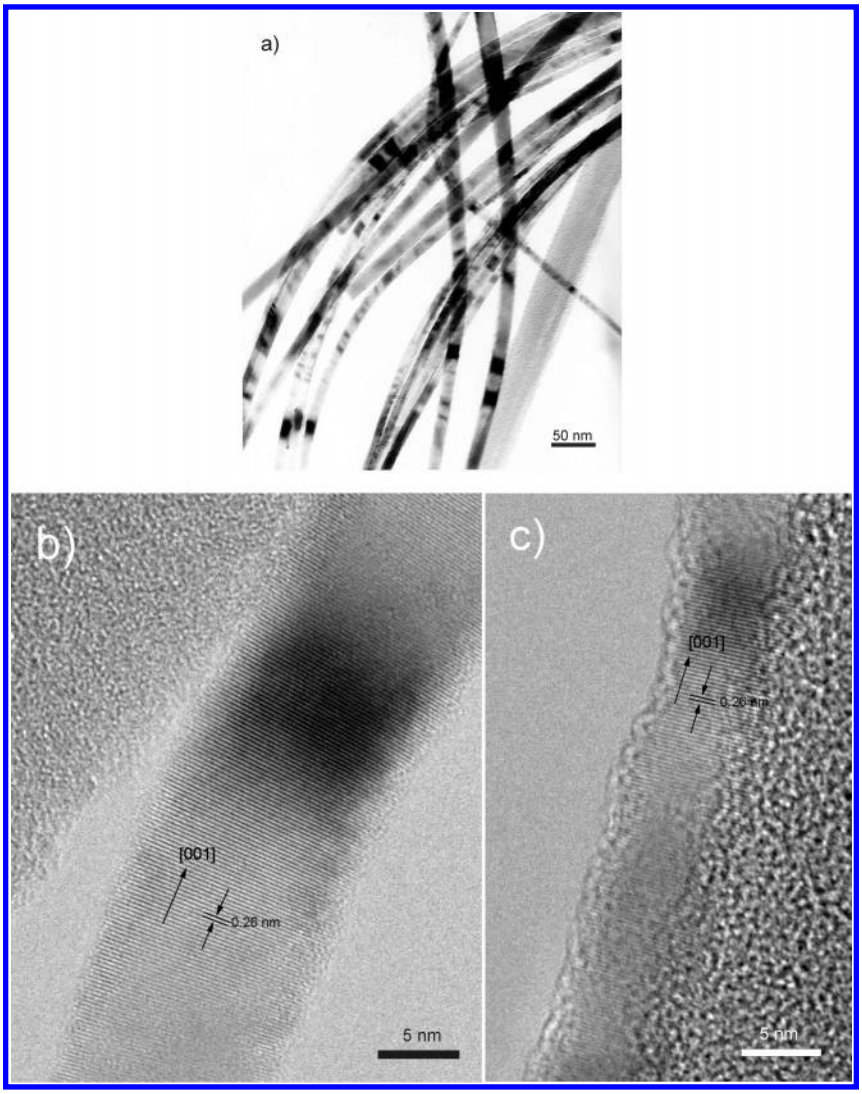

Figure 4. (a) TEM image of several ZnO nanowires, which have a similar diameter of around 15 nm. (b) HRTEM images of the body of a single ZnO nanowire and its tip part (c) showing (002) wurtzite planes and [001] growth direction.

The temperature range is also important for ZnO nanowire growth,[23] and the temperature range of 500−550 °C is desirable for nanowire growth. Only big ZnO particles were obtained at the lower temperature region (<500 °C) that is also farther away from the Zn source, due to a higher oxygen partial pressure (close to the open end of the tube). In the formation of ZnO nanoneedles and nanoflowers, the ratio of Zn to oxygen pressure is lower than when the Zn source was not covered. We believe it is the more limited Zn supply that leads to the nanoneedles cluster formation. At the slightly lower temperature region (500−530 °C), a low temperature and a higher oxygen partial pressure slow the needles growth to form a flowerlike structure. The reason for the formation of ZnO tubular whiskers at the contact region between the silicon cover and the tube is not clear; it is likely that this is due to a bottleneck effect. Because the ZnO tubular whiskers were only found in the contact area between the Si wafer and the Al_2O_3 crucible, the role of Al_2O_3 cannot be ruled out at present.[5]

X-ray excited optical luminescence (XEOL) from ZnO nanowires (Figure 2a), nanoneedles (Figure 2c), nanoparticles (Figure 2b), and bulk ZnO powder is shown in Figure 6a, where the area under the curve has been normalized to unity. There exist three regions of emission with a distinct near band-gap emission at 380. The branching ratio (area under the curve) of the intensities of the three regions, henceforth denoted band-gap (380 nm), defect (green luminescence peaked at 482 and 520 nm), and the second order of the near band-gap emission (760 nm), is shown in Figure 6b.

XEOL is a technique in which X-ray absorption produces core excitation, which results in holes in the valence band and electrons in the conduction band as well as defects in the excited state through a complicated energy-transfer process. The radiative recombination of electrons and holes leads to luminescence. At 1800 eV excitation energy, all of the core levels and valence band are excited with the exception of the Zn 1s shell (K-edge). The dominant process is the creation of the corehole in the Zn L shell and the O K-shell, which subsequently leads to holes in the valence band through core−hole decay and an electron in the bottom of the conduction band from thermalization.

From Figure 6, we see a strong emission at 380 nm. That UV band emission of ZnO corresponds to the near band-edge (3.37 eV band-gap) emission is well understood. Two strong emissions at 485 and 520 nm were observed only in the ZnO nanowire sample at the expense of the UV band emission. The green emission is often observed in ZnO and ZnO phosphors doped with activators. Recent studies attributed it to the singly ionized oxygen vacancy and the emission results from the recombination of electrons in singly occupied oxygen vacancies with photoexcited holes in the valence band (defect luminescence).[24] Because all of the nanostructures we prepared were

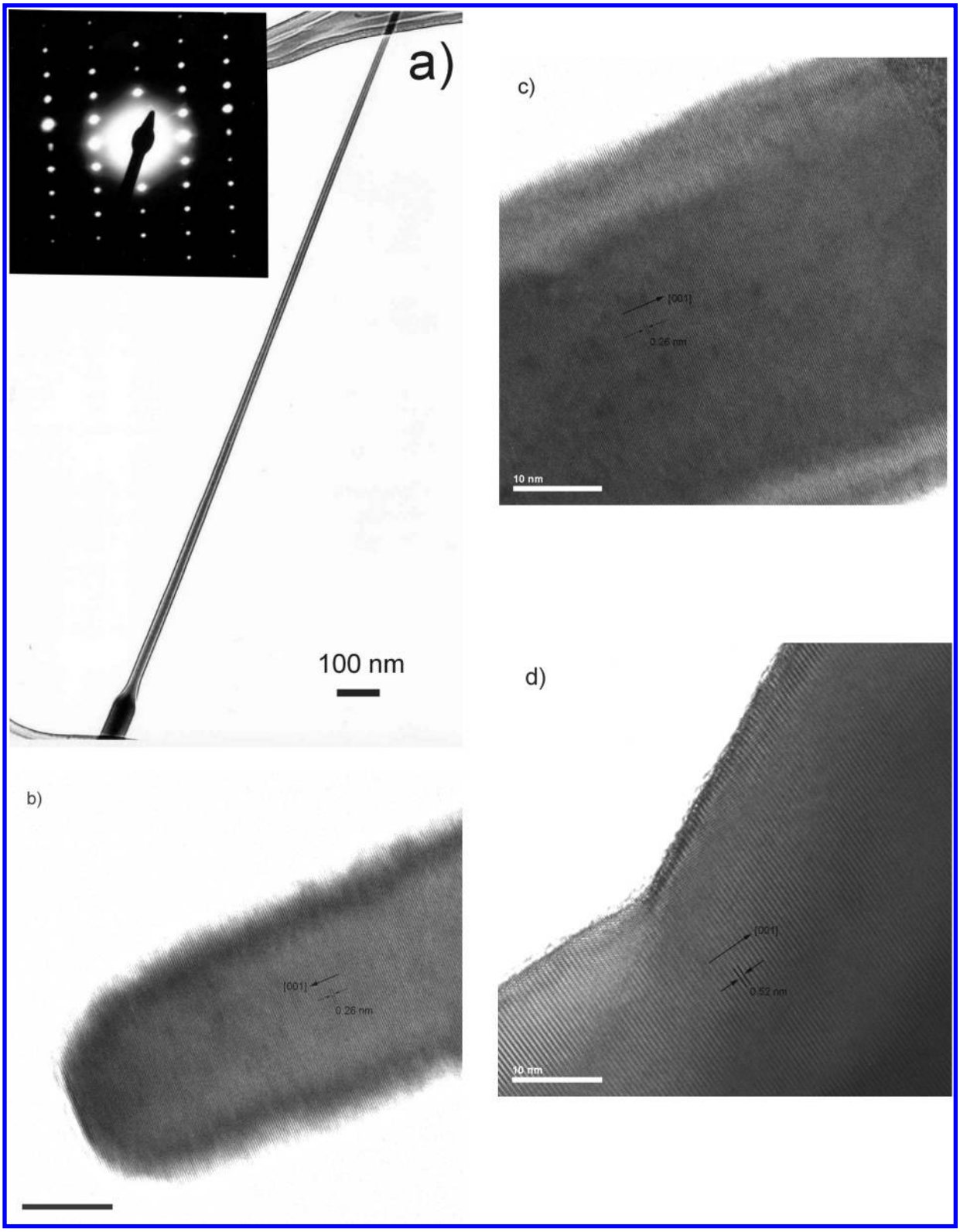

Figure 5. (a) TEM image of a single two-segment nanoneedle and its corresponding electron diffraction pattern (inset). HRTEM images of the tip (b), body of the upper segment (c), and connection part between the upper segment and the base segment (d).

from the same Zn source within the same furnace, we only see the green luminescence in the nanowire but not in the nanoneedle, we can rule out impurity activator as the source of the green luminescence. The intensity of the green band has been shown to be size-dependent such that the intensity increases as the wire diameter decreases.[25,26] This can also be seen in Figure 6b where the branching ratio of all of the emission is displayed. The green emission appears to be related to the crystallinity and the size. The TEM images clear show that the nanowire, which exhibits the more intense green light, has a rougher surface and interface as compared to the nearly perfect single crystal in the nanoneedle, which shows negligible green luminescence. As compared to nanoneedles, a higher surface area-to-volume ratio for the nanowires favors a higher level of surface oxygen vacancies. It should also be noted that the relative intensity of luminescence is nanowire > powder >

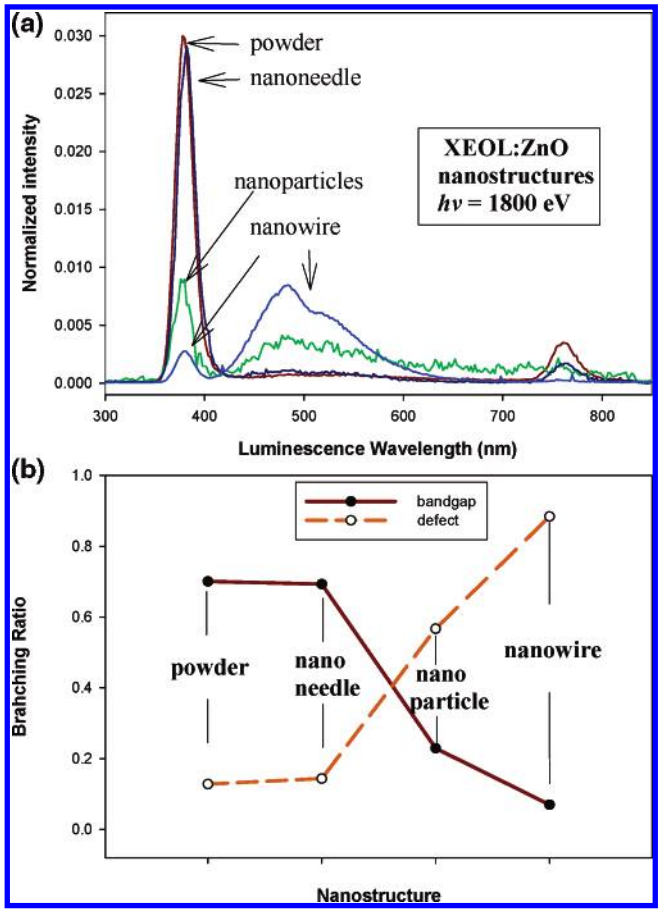

Figure 6. (a) XEOL spectra from ZnO nanowires, nanoneedles, nanoparticles, and bulk ZnO powder; the area under the entire spectrum has been normalized to unity. (b) The branching ratio of the band-gap and the green light (defect).

nanoneedle > nanoparticle. The luminescence intensity of the nanowire is at least 1 order of magnitude greater than the nanoparticle. The green light from the nanowire is so strong that it can be easily observed with the naked eyes when excited by a laboratory UV lamp.

In summary, we have reported the synthesis of a series of ZnO nanowires, nanoneedles, nanoflowers, and tubular whiskers, via the direct oxidation of Zn at 550 °C without the use of metal catalysts. All of these ZnO nanostructures have the same hexagonal wurtzite structure. ZnO nanowires are structurally uniform and have a similar diameter of around 15 nm and several micrometers in length. ZnO nanoneedles have a hexagonal tower structure, and the whole nanoneedle is a single crystal. Nanoflower was composed of hundreds of "nanopetals" which have a tadpole-like structure, and tubular whisker has a hexagonal hollow cone structure. We propose that the growth of ZnO nanostructures follows a vapor−solid (VS) growth process and the morphology depends on the ratio of Zn to oxygen partial pressure determined by the flow rate of Ar and the temperature. XEOL of ZnO nanostructures shows noticeable structure-dependent luminescence: ZnO nanowire has very strong green emission and relatively weak UV near band edge emission, while perfect single crystals of nanoneedles only show a UV near band edge emission. The strong green light emission is attributed to the defect involving an oxygen vacancy. We believe that this simple synthesis route will allow us to selectively fabricate specific ZnO nanostructure for various nanoscale device applications.

Acknowledgment. This work was supported by the Natural Science and Engineering Research Council (NSERC) of Canada. CSRF is supported by NSERC through a MFA grant and the National Research Council (NRC) of Canada. SRC is supported by the U.S. National Science Foundation under Grant DMR-00-84402. N.B.W. acknowledges the support of a grant from the Research Grants Council of Hong Kong SAR (SiNWs RGC Grant 9040879 (cityu 1024/03)). We thank Fred Pearson of the Brockhouse Institute for Material Research at McMaster University for his TEM technical assistance.

References and Notes

(1) Look, D. C. *Mater. Sci. Eng., B* **2001**, *80*, 383−387.
(2) Huang, M. H.; Mao, S.; Feick, H.; Yan, H. Q.; Wu, Y. Y.; Kind, H.; Weber, E.; Russo, R.; Yang, P. D. *Science* **2001**, *292*, 1897−1899.
(3) Geng, C. Y.; Jiang, Y.; Yao, Y.; Meng, X. M.; Zapien, J. A.; Lee, C. S.; Lifshitz, Y.; Lee, S. T. *Adv. Funct. Mater.* **2004**, *14*, 589−594.
(4) Greene, L. E.; Law, M.; Goldberger, J.; Kim, F.; Johnson, J. C.; Zhang, Y. F.; Saykally, R. J.; Yang, P. D. *Angew. Chem., Int. Ed.* **2003**, *42*, 3031−3034.
(5) Zhang, B. P.; Binh, N. T.; Wakatsuki, K.; Segawa, Y.; Yamada, Y.; Usami, N.; Kawasaki, M.; Koinuma, H. *Appl. Phys. Lett.* **2004**, *84*, 4098−4100.
(6) Wu, J. J.; Liu, S. C.; Wu, C. T.; Chen, K. H.; Chen, L. C. *Appl. Phys. Lett.* **2001**, *81*, 1312−1314.
(7) Hu, J. Q.; Bando, Y. *Appl. Phys. Lett.* **2003**, *82*, 1401−1403.
(8) Pan, Z. W.; Dai, Z. R.; Wang, Z. L. *Science* **2001**, *291*, 1947−1949.
(9) Yan, H. Q.; He, R. R.; Johnson, J.; Law, M.; Saykally, R. J.; Yang, P. D. *J. Am. Chem. Soc.* **2003**, *125*, 4728−4729.
(10) Kong, X. Y.; Wang, Z. L. *Nano Lett.* **2003**, *3*, 1625−1631.
(11) Gao, P. X.; Wang, Z. L. *Appl. Phys. Lett.* **2004**, *84*, 2883−2885.
(12) Yan, H. Q.; He, R. R.; Pham, J.; Yang, P. D. *Adv. Mater.* **2003**, *15*, 402−405.
(13) Dai, Y.; Zhang, Y.; Wang, Z. L. *Solid State Commun.* **2003**, *126*, 629−633.
(14) Arnold, M.; Avouris, P.; Pan, Z. W.; Wang, Z. L. *J. Phys. Chem. B* **2003**, *107*, 659−663.
(15) Li, Q. H.; Wan, Q.; Chen, Y. J.; Wang, T. H.; Jia, H. B.; Yu, D. P. *Appl. Phys. Lett.* **2004**, *85*, 636−638.
(16) Wan, Q.; Li, Q. H.; Chen, Y. J.; Wang, T. H.; He, X. L.; Li, J. P.; Lin, C. L. *Appl. Phys. Lett.* **2004**, *84*, 3654−3656.
(17) Bai, X. D.; Gao, P. X.; Wang, Z. L.; Wang, E. G. *Appl. Phys. Lett.* **2003**, *82*, 4806−4808.
(18) Hughes, W.; Wang, Z. L. *Appl. Phys. Lett.* **2003**, *82*, 2886−2888.
(19) Brenner, S. S.; Sears, G. W. *Acta Metall. Mater.* **1956**, *4*, 268.
(20) Wagner, R. S.; Ellis, W. C. *Appl. Phys. Lett.* **1964**, *4*, 89.
(21) Kitano, M.; Hamabe, T.; Maeda, S. *J. Cryst. Growth* **1990**, *102*, 965−973.
(22) Yao, B. D.; Chan, Y. F.; Wang, N. *Appl. Phys. Lett.* **2002**, *81*, 757−759.
(23) Kim, T. W.; Kawazoe, T.; Yamazaki, S.; Ohtsu, M.; Sekiguchi, T. *Appl. Phys. Lett.* **2004**, *84*, 3358−3360.
(24) Vanheusden, K.; Warren, W. L.; Seager, C. H.; Tallant, D. R.; Voigt, J. A.; Gnade, B. E. *J. Appl. Phys.* **1996**, *79*, 7983−7990.
(25) Yang, P. D.; Yan, H. Q.; Mao, S.; Russo, R.; Johnson, J.; Saykally, R.; Morris, N.; Pham, J.; He, R. R.; Choi, H. J. *Adv. Funct. Mater.* **2002**, *12*, 323−331.
(26) Shalish, I.; Temkin, H.; Narayanamurti, V. *Phys. Rev. B* **2004**, *69*, 245401.